CO 2 capture and CO 2 /CH 4 separation by silicas with controlled porosity and functionality

Saphir Venet, Frédéric Plantier, Christelle Miqueu, Ali Shahtalebi, Ross Brown, Thierry Pigot, Patrice Bordat

Version of Record: https://www.sciencedirect.com/science/article/pii/S1387181121007769
Manuscript_c769d0fd1500285c951a2fc9c7a35e0d

CO_2 capture and CO_2/CH_4 separation by silicas with controlled porosity and functionality

Saphir Venet[a,b], Frédéric Plantier[c], Christelle Miqueu[c], Ali Shahtalebi[c], Ross Brown[a], Thierry Pigot[a], Patrice Bordat[a,b,*]

[a] *Université de Pau et des Pays de l'Adour, E2S UPPA, CNRS, IPREM, Pau, France*
[b] *Université de Pau et des Pays de l'Adour, E2S UPPA, CNRS, TotalEnergies, LFCR, Pau, France*
[c] *Université de Pau et des Pays de l'Adour, E2S UPPA, CNRS, TotalEnergies, LFCR, Anglet, France*

Abstract

Microporous, mesoporous and hydrophobic silica materials with high specific surface area are obtained by an easy and cheap sol-gel synthesis. The effect of pore size and of water content on gas adsorption and separation are investigated. We also identified the relative amounts of different types of water in the porous silica, around 25% and 75% for bound and free water. The kinetics of rehydration is extremely slow, 60 % recovery after 4 days implying that the material can be used as is over several hours. Adsorption isotherms of pure gaseous CO_2 and CH_4, and of their mixtures at different pressures, show that among the materials synthesized, the microporous hydrophilic silica exhibits the best performance in terms of CO_2 adsorption capacity ($2.8\,mmol.g^{-1}$) and a separation factor over 10 at low CO_2 content and low pressure. Both properties are highly sensitive to the presence of residual water and to terminal chemical groups. This work highlights the possibility to develop competitive and cheap silica materials that could be scaled up to industrial uses.

Keywords:
CO_2 capture, CO_2/CH_4 separation, storage, porous silica, water, sol-gel synthesis, CCS

* *Email address:* patrice.bordat@univ-pau.fr (Patrice Bordat)

Introduction

CO_2 emissions from human activities [1] are recognised as the main contribution to the constant increase of atmospheric carbon dioxide (CO_2) responsible for global warming [2, 3]. CO_2 capture and storage technologies (CCS) are widely explored to mitigate the increasing concentration of CO_2. Adsorption processes are among the most promising techniques for separating CO_2 from exhaust gases [4]. Finding suitable adsorbents with a large storage capacity and selectivity for CO_2 nonetheless remains challenging.

Much work focused on the capture of atmospheric CO_2, for which CO_2/N_2 adsorption efficiency and selectivity are crucial. Carbon-based materials were developed with an optimal content of mono- or multi-hetero atoms like N, S, O in order to maximize the CO_2 adsorption capacity[5, 6]. These materials, combining nitrogen hetero-atoms and microporosity mainly below 0.73 nm achieved CO_2 adsorption over 6.4 $mmol.g^{-1}$. Other studies have focused on both CO_2 adsorption and CO_2/N_2 selectivity[7, 8, 9], finding that multi-hetero atoms improve CO_2 adsorption as well as CO_2/N_2 selectivity. In these hetero-atom basic Lewis sites induce affinity for CO_2 while narrow pores discriminate the smaller kinetic radius of CO_2 relative to N_2.

Separation of CO_2 from CH_4 is also important, *e.g.* in many industrial processes such as natural gas sweetening (*e.g.* CO_2 removal from high pressure methane in natural gas wells), biogas upgrading [10], oil recovery enhancement and landfill gas purification [11]. Developing cheap, efficient techniques for removal fand capture of CO_2 in CH_4, over a wide range of CO_2 concentrations and flow rates is thus important. One promising way to achieve this goal is the use of porous materials [12, 13], *e.g.* Many of them are considered as potential candidates for CO_2 capture as for example, zeolites (5A and 13X) [14], activated carbon [15, 16], mesoporous silica (SBA-15, MCM-41, ...) [17, 18, 19], silica gel [20] and metal organic frameworks[21, 22]. Earlier work showed that CO_2 adsorption performance stems from the combined effects of microporosity and functionalization, again mainly with basic nitrogen functions[23, 24]. Moreover, it is well-known that nitrogen functions efficiently capture CO_2 *via* a chemisorption phenomenon leading to high costs for the regeneration of the materials [25, 26]. We prefer to design an efficient porous silica material favouring physisorption in order to facilitate its regeneration.

Here we report on synthesis and characterisation of silica adsorbants for CO_2/CH_4 separation, rationalising and optimising the main parameters in-

fluencing the CO_2 adsorption efficiency from gaseous mixtures. We do not use nitrogen functions in order to preserve easy, cheap regeneration of the materials, based on CO_2 physisorption. In particular, we examine the effects of micro- *vs.* mesoporosity, by changing the synthesis pH, and the kinds and amounts of water- free or bound to silica, by modifying the hydrophilicity or hydrophobicity *via* partial methylation. Understanding the role of water is important since it will be present under practical conditions such as temperature under which separation of CO_2 and CH_4 is to be achieved.

1. Materials and Methods

Synthesis

Materials are synthesized by sol-gel route from the precursor tetramethoxyorthosilicate (TMOS). Molar ratios are 1/5/4 for alkoxide, methanol and water. The general synthesis protocol used by our group, originaly for a completely different application, is described by C. Cantau *et al.* [27]. Two synthesis strategies are developed here: *(i)* modifying the pH to control the porosities; *(ii)* use of a second precursor, trimethoxymethylsilane (TMMS), to induce a degree of hydrophobicity, as summarized in Table 1. Xerogels are dried 10 days at 60°C, 10 days at 30°C, 6 hours at 60°C and finally 2 days at 80°C.

Material	S_{ref}	S_{pH9}	S_{TMMS}
Precursor	TMOS	TMOS	60% TMOS + 40% TMMS
Synthesis pH	6	9	6
Characteristics	Microporous hydroxylated	Mesoporous hydroxylated	Microporous partially methylated
Physisorbed water (wt%)	11	8	5
Hydroxyl groups (wt%)	5	4.5	9^a
Organic matter (wt%)	2	1	
Specific surface area($m^2.g^{-1}$)	700	580	$85/250^b$
Free water fraction (%)	75	76	73
Bound water fraction (%)	27	24	27
Ratio	2.7	3.2	2.7

Table 1: **Synthesis conditions and properties of the present materials.** *a.* sum of hydroxyls and organic matter. *b.* Second value refers to CO_2 adsorption.

Characterisation

Several experimental techniques are applied to characterize the materials, particularly adsorbed water, see the SI for details. Diffuse reflectance infra-red Fourier transform (DRIFT) is used to track the influence of heat treatment *via* I.R. band intensities relative to the 1100 cm^{-1} band of the silica matrix. We probed material texture *via* N_2 adsorption isotherms and thermogravimetric analysis (TGA). We probe different types of adsorbed water, *e.g.* during rehydration of S_{ref}, by near infra-red spectroscopy (NIR), decomposing spectra in the 4700–5500 cm^{-1} range into a sum of gaussian contributions. Adsorption of pure and mixed gases is quantified by recodring gravimetric or barostatic adsorption isotherms.

2. Results and discussion

Diffuse Reflectance Infrared Fourier Transform Spectroscopy

Fig. 1 shows the DRIFT spectra of the three kinds of silica. The dominant 1100 cm^{-1} band and broad shoulder at 1170 cm^{-1} (ν_{anti}(Si-O-Si) asymmetric stretch) attest formation of the Si-O-Si framework in all the materials, while the band at 940 cm^{-1} is due to Si-OH groups (ν(Si-OH) stretch)[28, 29]. The 800 cm^{-1} band is variously attributed in the literature to the δ(Si-OH) deformation[28] or to the symmetrical ν_s(Si-O-Si) stretch[29, 30]. Here, we find the band is unchanged in heated samples, indicating that it is due to ν_s(Si-O-Si) stretching. The hydroxyl stretching band is due to incomplete condensation during synthesis, while the weak but significant bands around 1400 cm^{-1} and 2900 cm^{-1}, attributed in refs. [29, 31] to δ(-CH_3) deformation and ν(-CH_3) elongation of methyl groups linked to a silicon atom, imply incomplete hydrolysis. The overall formula of the materials is thus $(SiO_{2-y-z})_x(OH)_y(OCH_3)_z$ with y and z small compared to x. The spectrum of the S_{pH9} material (black curve) differs only by the intensity of the bands relative to the reference material S_{ref}.

Compared to the reference spectrum (blue), the spectrum of material prepared with 40 % of the methylated precursor shows additional bands (red curve): an antisymmetic Si-CH_3 stretching mode at 2960 cm^{-1}, Si-CH_3 stretching at 2870 cm^{-1}, antisymmetric -CH_3 deformation at 1450 cm^{-1}, and -CH_3 symmetric deformation at 1370 cm^{-1}[31]. The spectrum indicates a silica network with both surface hydroxyl and terminal CH_3 groups.

Water and surface hydroxyl groups in the materials appear in the range 3000–3800 cm^{-1}. Thus the broad water stretch band, peaking at 3300 cm^{-1},

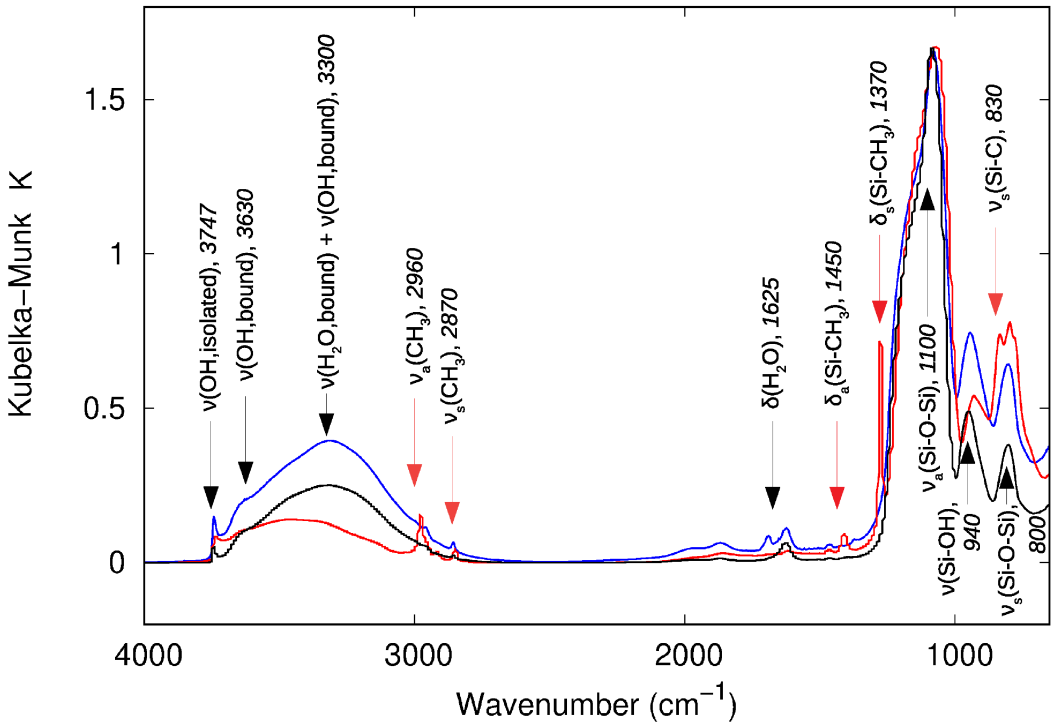

Figure 1: **Main IR bands of the as synthesized materials.** DRIFT spectra of: S_{ref} (blue), S_{pH9} (black) and S_{TMMS} (red), with assignments and positions in cm^{-1}. Spectra are normalized on the silica network band at $1100\,\text{cm}^{-1}$.

decreases on heating the materials and disappears beyond 400°C, see *e.g.* supplementary Fig. 3. The shoulder at 3630 cm^{-1} is due to stretching of hydroxyl groups engaged in hydrogen bonds with water or between vicinal surface silanols[32, 30]. The sharply peaked free hydroxyl stretching band at 3747 cm^{-1} indicates isolated or geminal silanols without any interaction with water[32, 30]. Here, it indeed becomes relatively more prominent on heating, as more and more water or hydroxyls are desorbed. Conversely the characteristic bending mode of water[32, 30] around 1625 cm^{-1} disappears on heating the sample, supplementary Fig. 3.

Thermogravimetric analysis (TGA)

TGA, see Fig. 2, quantifies physisorbed water, the density of surface hydroxyls and organic residues such as those left by incomplete hydrolysis. The first, sharp drop, 11 % for the reference sample at 150 °C corresponds to loss of physisorbed water. It is followed by a slower drop up to 400 °C, as surface silanols are driven off, 5 % for S_{ref} after accounting for 2 % loss of organic matter at 400 °C. Dehydroxylation is still incomplete at 800 °C, making the water contents in table 1 lower bounds. Considering the high organic content of the methylated silica, we report only a net weight loss beyond 150 °C.

N_2 isotherms for textural characteristics

Table 1 reports the porosity data deduced from the N_2 adsorption isotherms shown in Fig. 3. As an indication, the specific surface area of S_{ref} varied between 600 and 800 $m^2.g^{-1}$ between synthesis batches. The isotherm of this material is type I(b), with some of the character of type IV, indicating firstly a wide distribution of pore sizes, including micropores and possibly narrow mesopores, and secondly the presence of a small amount of mesopores. A quite different, type IV isotherm with clear hysteresis indicates a majority of mesopores in S_{pH9}. However, the similarity of the S_{pH9} and S_{ref} isotherms at low very pressure implies comparable microporosities, consistent with the lower specific area of S_{pH9} compared to S_{ref} (table 1). The surprisingly low specific surface area of S_{TMMS} would suggest a non-porous material, but the area deduced from CO_2 adsorption (*cf.* inset of Fig. 3) is nonetheless 225 $m^2.g^{-1}$. The smaller kinetic diameter of CO_2, compared to that of N_2 [8, 9], may explain this result, then implying the presence of ultra-micropores (*cf.* [8, 9]).

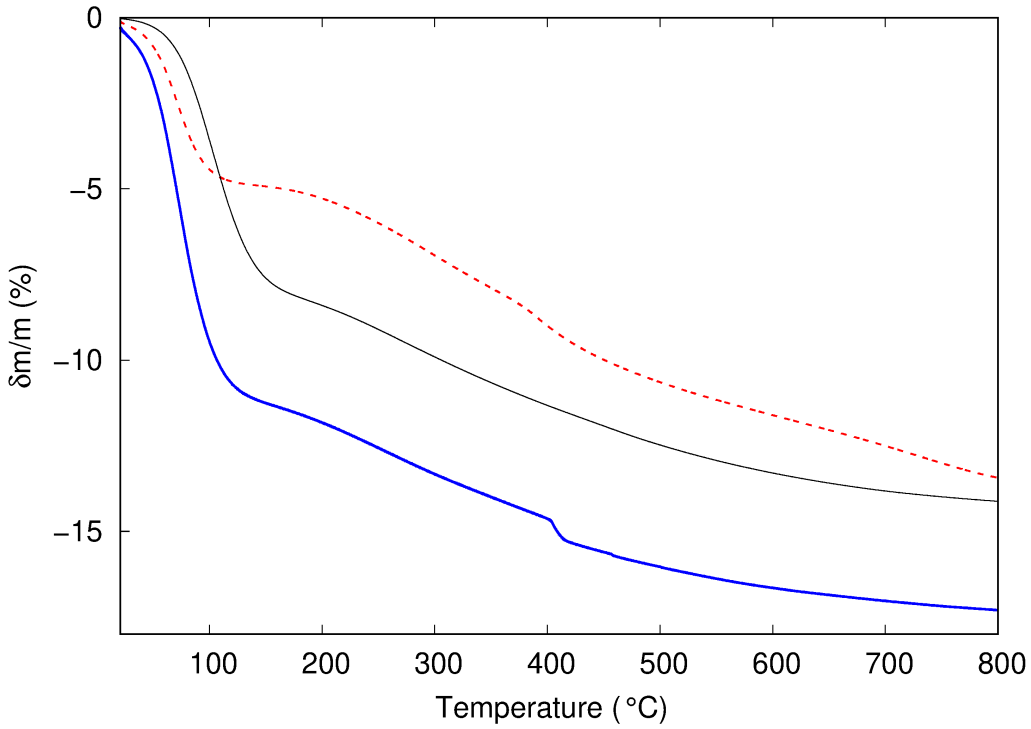

Figure 2: **Loss of water, hydroxyls and organic matter.** Thermogram of S_{ref} (blue thick line), S_{pH9} (black thin line) and S_{TMMS} (red dotted line).

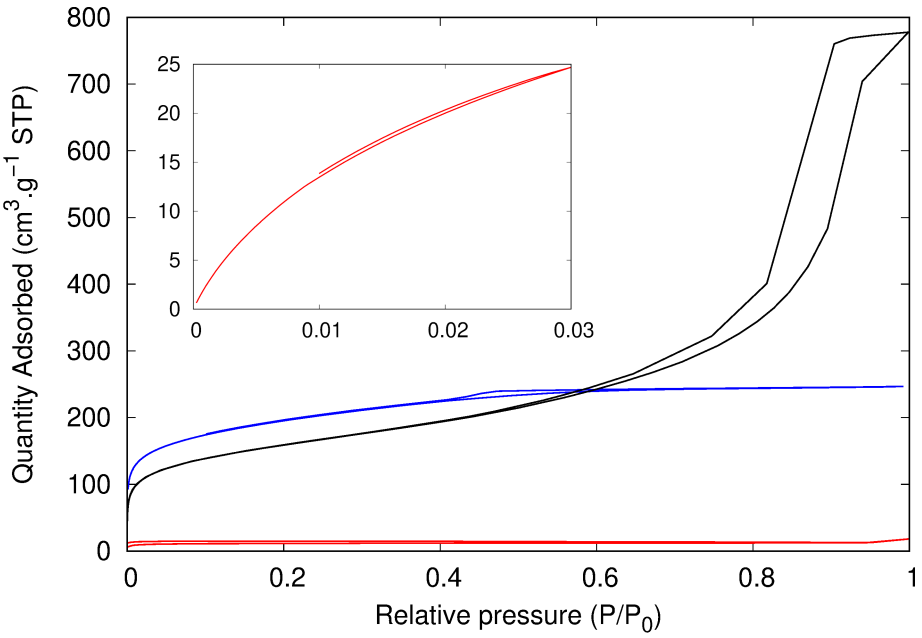

Figure 3: N_2 isotherms of S_{ref} (blue), S_{pH9} (black) and S_{TMMS} (red). inset: adsorption and desoprtion of CO_2 for S_{TMMS} only.

Surface density of hydroxyls

Except for S_{TMMS}, where the organic matter strongly screens the surface, we determine the total number of hydroxyl groups from the mass of water lost Δm during the second stage of TGA and the relation[30]:

$$N_{\text{OH}} = \frac{2\Delta m \times N_{\text{A}}}{M_w} \quad , \tag{1}$$

where M_{w} is the molecular weight of water, N_{A} is Avogadro's number and the factor 2 accounts for the formation of one water molecule per 2 silanols. Combining values with the specific surface areas, we find the density of surface hydroxyls, $\sigma_{\text{OH}} = 4.8$ and $5.2\,\text{nm}^{-2}$ for S_{ref} and S_{pH9}. Considering the estimated 15 % uncertainty in the specific surface areas, the materials are equally hydrophilic and are also representative amorphous silicas, for which the average silanol density is $4.6\,\text{nm}^{-2}$[33]. Obviously, some inhomogeneity of the distribution of adsorbed water is to be expected. Thus, although the $\times 2$ ratio between the first and second weight losses under TGA is consistent with a complete surface monolayer of water, with one donating and one

receiving hydrogen bond on every silanol, confirming or contradicting this simple picture requires other information, provided by NIR spectroscopy.

Near-infrared spectroscopy (NIR)

Relative intensities of the water band $\approx 3500\,\mathrm{cm}^{-1}$ in the DRIFT spectra of Fig. 1 are consistent with the corresponding specific surface areas, but this band contains contributions from silanols and does help distinguish bound from bulk water. We therefore recorded NIR spectra, basing our interpretation of physisorbed water on the assignment of hydroxyl stretching and water bending combination bands around $5200\,\mathrm{cm}^{-1}$ in ref. [34], *e.g.* *(i)* a band at $5270\,\mathrm{cm}^{-1}$ due to water on (geminal) silanols; *(ii)* a band at $5180\,\mathrm{cm}^{-1}$ in bulk water, assigned to combination of ν_2 ($1644\,\mathrm{cm}^{-1}$) and ν_3 ($3490\,\mathrm{cm}^{-1}$).

Comparison of the spectra of S_{ref} before drying under vacuum at 120 °C, and during rehydration, assists assignment in Fig. 4a. The as synthesised sample shows an asymmetrical peak at $5200\,\mathrm{cm}^{-1}$, with a clear shoulder on the lower energy side, and a broad double peak around $7000\mathrm{cm}^{-1}$ (blue curve). On drying (black curve), the $\approx 5200\,\mathrm{cm}^{-1}$ band in agreement with ref.[34] resolves into a mean peak at $\approx 5250\,\mathrm{cm}^{-1}$ and a low energy shoulder around $5150\,\mathrm{cm}^{-1}$. The massif at $7000\,\mathrm{cm}^{-1}$ transforms into a peak at $7317\,\mathrm{cm}^{-1}$ and two low energy shoulders. In agreement with ref. [34], we interpret the sharp peak at $7317\,\mathrm{cm}^{-1}$ as silanols freed by drying, the first shoulder ($7121\,\mathrm{cm}^{-1}$) as water coordinated silanols and the second ($6861\,\mathrm{cm}^{-1}$) as bulk water. Consistent with this, the intensities of the shoulders relative to the sharp peaks recover during rehydration. Recovery is slow, *e.g.* the last spectrum was recorded 4 days after dessication.

Deconvolution of the ≈ 5200 band in all the as synthesised samples then provides the proportions of bound and bulk water before drying, see table 1, and the SI for details. Note that although the total amount of water depends on the synthesis, the proportions of free (or bulk) and bound water are the same in all the samples, $\approx 3:1$, suggesting that water in S_{TMMS} is confined to un-functionalised areas of the porous network. Using the specific surface areas, and first and second weight losses in TGA above, we deduce that on average, 1 in 4 silanols in S_{ref} hosts a water molecule, and 1 in 5 in S_{pH9}.

Employing the same spectral decomposition, we can follow rehydration of dried silica exposed to ambient air. Fig. 4b shows the initial 0-order recovery kinetics of free and bound water in dessicated S_{ref}. After 4 days, the recovery of bound water has clearly slowed down (characteristic time 2.5 days in the dashed-line fit to an exponential saturation model, see the SI), whereas the

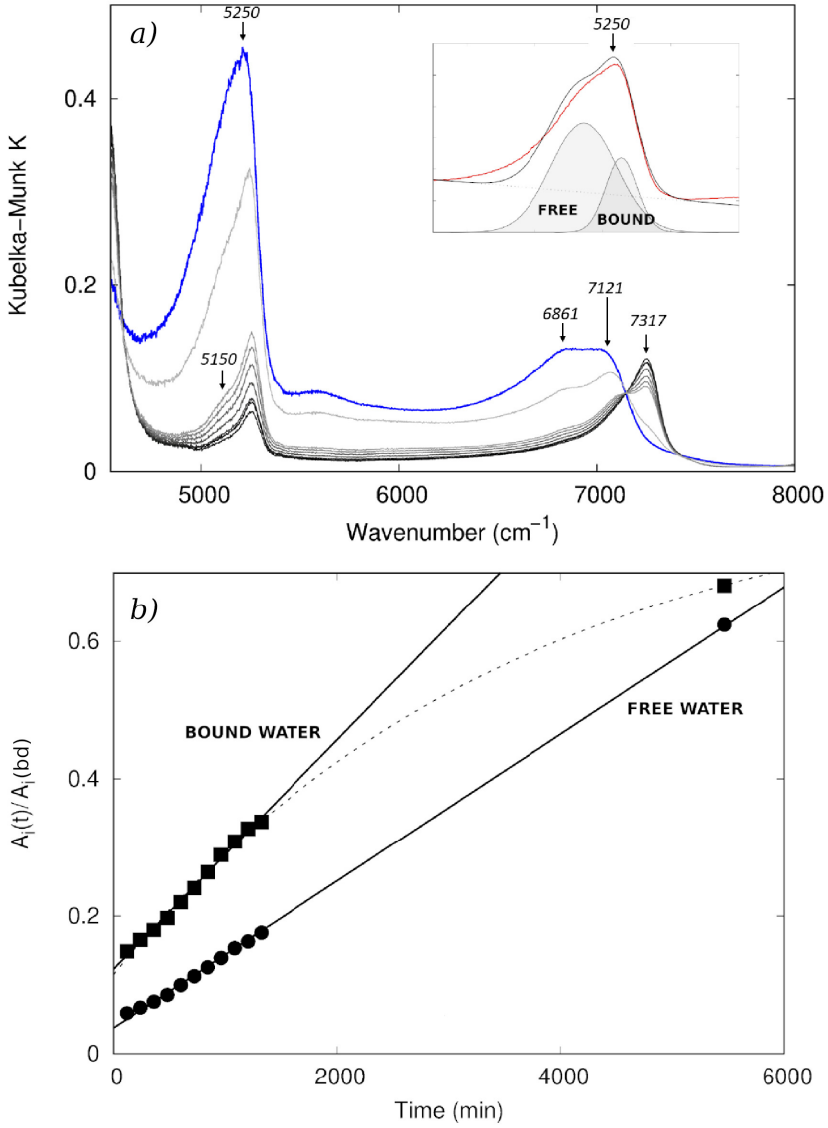

Figure 4: **NIR monitoring of rehydration (ambient conditions) of $S_{\mathbf{ref}}$ silica, vacuum-dried at 120 °C, assists identification of the physisorbed and bulk water in ambient conditions.** *(a)* Spectra are shown as synthesised before dessication (blue) and during rehydration (black to light grey). Inset: exemple of deconvolution of the experimental spectra into two gaussian contributions. *(b)* Recovery of bound and free water under ambient conditions, from the deconvolution (See SI). $A_i(t)$ i=bound or free, is the area of component i at time t and $A_i(bd)$ is the corresponding area before drying. Straight lines show initial zero-order kinetics (rate constants $k_{\text{bound}} \approx 1.7 \times 10^{-4}\,\text{min}^{-1}$ and $1.1 \times 10^{-4}\,\text{min}^{-1}$; dashed line: exponential fit to the tailing off of recovery of bound water (see the SI), with characteristic time $\tau_{\text{R}} = 60\,\text{h}$.

contribution of free water continues to recover at its initial rate. One possible explanation would congestion due to already adsorbed water in narrow pores, *cf.* the type I(b) isotherm in Fig. 3.

The above results, show that dessicated S_{ref} is not fully dehydrated under the conditions described, and small amounts of residual water may influence gas adsorption. The slowness of redyhdration may prove an advantage in applications since it makes drying the gaseous mixture to be separated less important.

Gas adsorption

CO_2 adsorption by S_{ref} is improved by pre-baking the as synthesised material under vacuum, see supplementary Fig. 1 and discussion in the SI. The adsorption capacity increases with the baking temperature, but only marginally above 80 °C. Because we find below that leaving some adsorbed water is actually favourable to CO_2 adsorption, and because baking at higher temperatures may drive off some silanols[33], we pre-baked all samples at 80 °C.

Fig. 5 shows the adsorption isotherms of pure CO_2 or CH_4. The mesopororous silica S_{pH9} has the highest capacity for either pure gas. All the silicas adsorb more CO_2 than CH_4 as measured by the ratio of the amounts absorbed from each gas taken separately, $R = n^{\mathrm{a}}_{\mathrm{CO_2}}/n^{\mathrm{a}}_{\mathrm{CH_4}}$ (commonly called the selectivity for gas mixtures), *cf.* Table 2. As well known, and expected here, microporosity favours CO_2 adsorption relative to CH_4. Thus, although S_{pH9} has the highest capacity for either gas, S_{ref} has the best selectivity over the present range of pressures. Ultra-microporosity is known [5, 6] to enhance the adsorption capacity of CO_2, but here the lower adsorption capacity of S_{TMMS} probably is due to its lower specific surface area.

Less expectedly, table 2 also shows that S_{TMMS} does not perform as well as S_{ref}. The initial assumption was that partial methylation would improve CO_2 adsorption capacity by reducing competition with adsorption of water. But, partial methylation, leads to stronger competition with CH_4 adsorption, and in fact lower selectivity than determined for S_{ref}. Moreover, the low specific surface area found for S_{TMMS} induces a lower adsorption capacity for both gases. Thus, partial methylation is not the best way to improve both the adsorption capacity and the selectivity.

Silica S_{ref} has nearly the same capacity as S_{pH9}, but is more selective. Therefore, we measured adsorption isotherms of CO_2/CH_4 mixtures only on

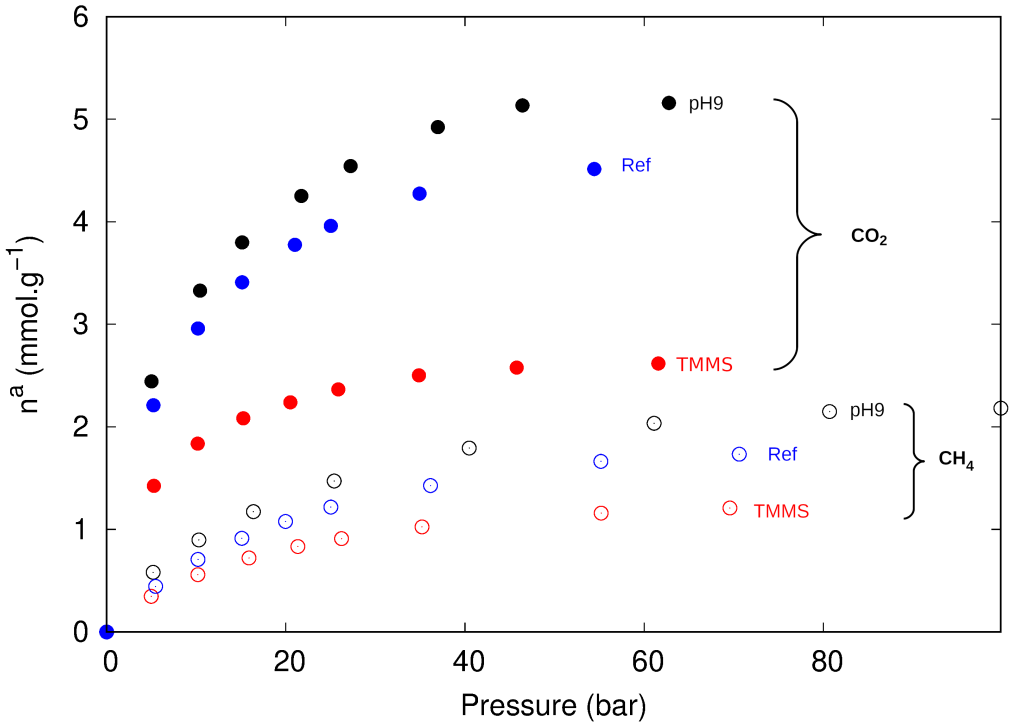

Figure 5: **Methylation reduces adsorption capacity for both pure gases.** Adsorption isotherms of pure CO_2 (•) and pure CH_4 (○) for the S_{ref} (blue), S_{pH9} (black) and S_{TMMS} silicas (red). Capacity for CO_2 relative to CH_4 is greater at lower pressure, see Table 2.

Silica material	$R_{5\,\text{bar}}$	$R_{55\,\text{bar}}$
S_{ref}	5	2.7
S_{pH9}	4.1	2.2
S_{TMMS}	4.2	2.5

Table 2: **Greater CO_2 than CH_4 adsorption at low pressure by S_{ref}.** The ratio of the amounts adsorbed from either gas separately, $R_p = n^a_{CO_2}/n^a_{CH_4}$, *cf.* Fig. 5 for S_{ref}, S_{pH9} and S_{TMMS} at low and high pressure.

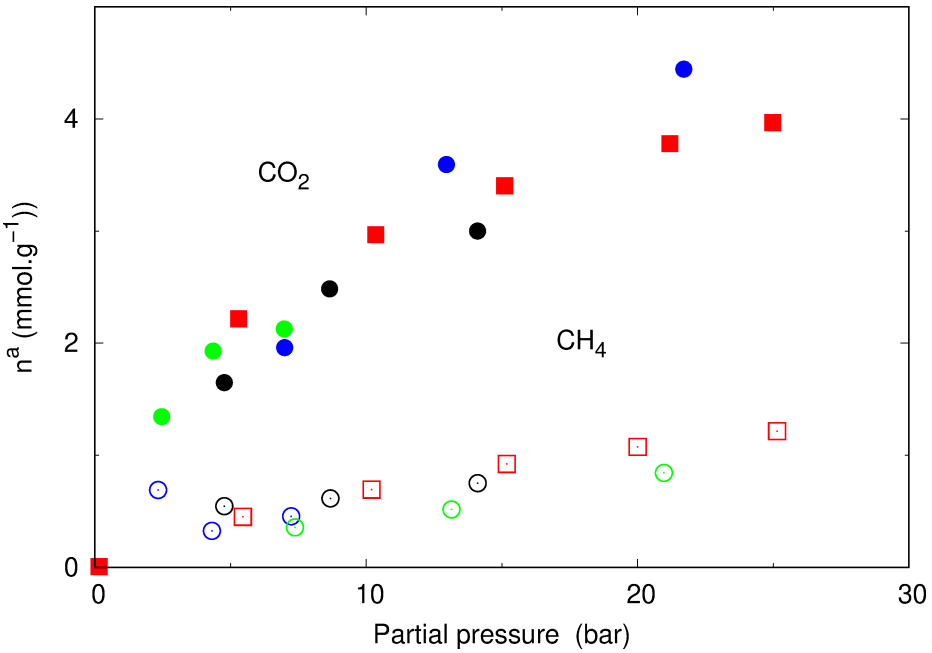

Figure 6: **Silica $S_{\mathbf{ref}}$ is $\mathbf{CO_2}$-selective.** Specific adsorbance (n^{a}) of CO_2 exceeds that of CH_4, even from CH_4-rich mixtures. Simultaneous adsorption isotherms of CO_2 (•) and CH_4 (○) from CO_2/CH_4 gas mixtures in the proportions: 25/75 (green), 50/50 (black) and 75/25 (blue) v/v; red squares: pure gases (*cf.* Fig. 5).

S_{ref}. The plot of specific adsorptions, n_{a}, against partial pressures in Fig. 6 shows that to within experimental accuracy the amounts adsorbed depend only on the partial pressures, with significant selection of CO_2.

Fig. 7 shows another common way of representing selective adsorption, the separation factor,

$$SF = \frac{x_{\mathrm{CO_2}}/x_{\mathrm{CH_4}}}{y_{\mathrm{CO_2}}/y_{\mathrm{CH_4}}} \quad , \tag{2}$$

where x_i is the molar fraction of adsorbed species i and y_i the molar fraction in the equilibrated gas above the adsorbent, see the SI. Material S_{ref} achieves high SF for CO_2 *vs.* CH_4 at compositions representative of raw biogas *e.g.* CO_2 fraction between and 10 and 50 % and pressure under 20 bar.

Therefore, the best compromise between the adsorption capacity and the separation factor is obtained for a CO_2 composition below 30% and a pressure below 20 bars.The adsorption capacity of CO_2 can then be as high as

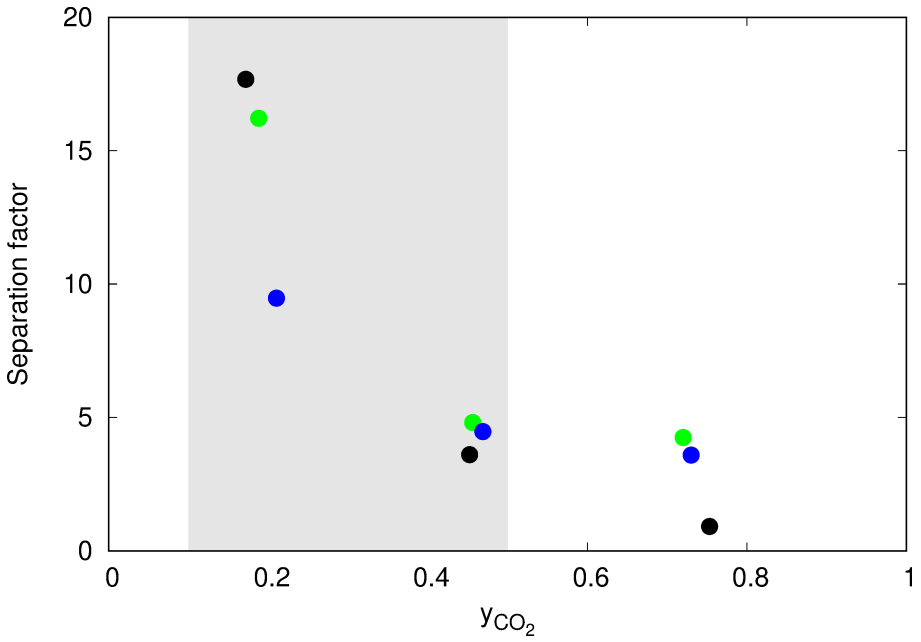

Figure 7: **Efficient separation ability especially at low CO_2 content and moderated pressures.** Separation factors of S_{ref} *vs.* the gas phase fraction of CO_2 for 3 different pressures. 10 bar (black), 17 bar (green) and 28 bar (blue). Grey rectangle: typical biogas application range.

Adsorbant	CO_2/CH_4 adsorption $mmol.g^{-1}$	Selectivity	Experimental conditions	Type of porosity
Present work, S_{ref}	2.8 / 0.7	4	10 bars, 303K	Micro-
NaX Zeolite[35]	6 / 3.2	1.9	1 bar, 303K	Micro-
MAXSORB-III[36]	10 / 5.6	1.8	1 bar, 300K	Meso-
5A Zeolite[37]	3.6 / 2	1.8	10 bar, 303K	Micro-
AC ROx 0.8 [38]	4 / 1.6	2.5	10 bar, 303K	Micro-
MCM-41[39]	4.5 / 1.2	3.7	1 bar, 298K	Meso-
MOF-200/GO [40]	1.34 / 0.20	6.7	1 bar, 298K	Micro-meso-macro
MMM SSZ-16 [41]	2.28 / 0.35	6.5	1 bar, 298K	Micro-
K-Rho Zeolite[42]	3.7 / 0.04	92	10 bar, 298K	Meso-

Table 3: **S_{ref} combines moderate adsorption capacity and good selectivity in an easily synthesised and cheap material compared to well-known ones.** Comparison of S_{ref} with materials commonly used to separate CO_2 and CH_4.

2.8 mmol.g^{-1} *vs.* only 0.7 mmol.g^{-1} for CH_4, and the separation factor can exceed 15. While several materials in the literature perform better for one or other metric, *e.g.* MOF-200/GO for selectivity but not for adsorption capacity, or MAXSORB-III for the reverse combination, see table 3, S_{ref} combines here moderate adsorption capacity and fair to high selectivity in an easy, cheap synthesis, not the case for MMM SSZ-16 for example.

3. Conclusion

The present easy and cheap sol-gel synthesis leads to microporous to mesoporous amorphous silica materials with different water affinity, aimed here at CO_2/CH_4 separation. They were characterized by several experimental techniques in order to establish their composition, porosity and water content, specially free and bound water and rehydration kinetics.

The mesoporosity and possibly the slightly higher surface density of hydroxyls in S_{ph9} lead to greater CO_2 adsorption capacity, but at the expense of selectivity which is greatest in microporous S_{ref}, which attains a selectivity of 4 and a separation factor over 15 in CO_2-poorer CO_2/CH_4 mixtures at low pressures. Contrary to expectation, we find a degree of residual water in S_{ref} is favorable to CO_2 adsorption at higher pressures. Thus, peak adsorption of CO_2 requires only moderate heating (80 °C) to drive off atmospheric and residual synthesis water before use or to regenerate the material. Furthermore, rehydration under ambient conditions is slow, some hours. Considering the facile and cheap synthesis, the material thus appears promising for applications like natural gas sweetening or biogas upgrading.

Acknowlegment

This work was funded by the ISIFoR Carnot Institute (sustainable engineering of georesources). We thank S. Labat, S. Blanc and J. P. Grenet for their help in experimental work and M. Le Bechec for help and useful discussions.

References

[1] G. Singh, J. Lee, A. Karakoti, R. Bahadur, J. Yi, D. Zhao, K. AlBahily, A. Vinu, Emerging trends in porous materials for co2 capture and conversion, Chem. Soc. Rev. 49 (2020) 4360–4404. doi:10.1039/D0CS00075B.

[2] T. Root, J. Price, K. Hall, S. Schneider, C. Rosenzweig, A. Pounds, Fingerprints of global warming on wild animals and plants, Nature 421 (2003) 57–60. doi:10.1038/nature01333.

[3] D. Y. Leung, G. Caramanna, M. M. Maroto-Valer, An overview of current status of carbon dioxide capture and storage technologies, Renewable and Sustainable Energy Reviews 39 (2014) 426–443. doi:10.1016/j.rser.2014.07.093.

[4] S.-Y. Lee, S.-J. Park, A review on solid adsorbents for carbon dioxide capture, Journal of Industrial and Engineering Chemistry 23 (2015) 1–11. doi:10.1016/j.jiec.2014.09.001.

[5] A. Rehman, Y.-J. Heo, G. Nazir, S.-J. Park, Solvent-free, one-pot synthesis of nitrogen-tailored alkali-activated microporous carbons with an efficient CO_2 adsorption, Carbon 172 (2021) 71–82. doi:10.1016/j.carbon.2020.09.088.

[6] G. Nazir, A. Rehman, S.-J. Park, Sustainable n-doped hierarchical porous carbons as efficient CO_2 adsorbents and high-performance supercapacitor electrodes, Journal of CO_2 Utilization 42 (2020) 101326. doi:10.1016/j.jcou.2020.101326.

[7] G. Nazir, A. Rehman, S.-J. Park, Valorization of shrimp shell biowaste for environmental remediation: Efficient contender for CO_2 adsorption and separation, Journal of Environmental Management 299 (2021) 113661. doi:10.1016/j.jenvman.2021.113661.

[8] G. Nazir, A. Rehman, S.-J. Park, Role of heteroatoms (nitrogen and sulfur)-dual doped corn-starch based porous carbons for selective CO_2 adsorption and separation, Journal of CO_2 Utilization 51 (2021) 101641. doi:10.1016/j.jcou.2021.101641.

[9] A. Rehman, G. Nazir, K. Yop Rhee, S.-J. Park, A rational design of cellulose-based heteroatom-doped porous carbons: Promising contenders for CO_2 adsorption and separation, Chemical Engineering Journal 420 (2021) 130421. doi:10.1016/j.cej.2021.130421.

[10] O. Awe, Y. Zhao, A. Nzihou, D. Pham Minh, N. Lyczko, A review of biogas utilisation, purification and upgrading technologies, Waste and Biomass Valorization 8 (2017). doi:10.1007/s12649-016-9826-4.

[11] H. Yang, Z. Xu, M. Fan, R. Gupta, R. B. Slimane, A. E. Bland, I. Wright, Progress in carbon dioxide separation and capture: A review, Journal of Environmental Sciences 20 (2008) 14–27. doi:10.1016/S1001-0742(08)60002-9.

[12] A. Modak, S. Jana, Advancement in porous adsorbents for post-combustion CO_2 capture, Microporous and Mesoporous Materials 276 (2019) 107–132. doi:10.1016/j.micromeso.2018.09.018.

[13] B. Petrovic, M. Gorbounov, S. Masoudi Soltani, Influence of surface modification on selective CO_2 adsorption: A technical review on mechanisms and methods, Microporous and Mesoporous Materials 312 (2021) 110751. doi:10.1016/j.micromeso.2020.110751.

[14] S. Garcés-Polo, J. Villarroel-Rocha, K. Sapag, S. Korili, A. Gil, A comparative study of CO_2 diffusion from adsorption kinetic measurements on microporous materials at low pressures and temperatures, Chemical Engineering Journal 302 (2016) 278–286. doi:10.1016/j.cej.2016.05.057.

[15] M. Plaza, S. García, F. Rubiera, J. Pis, C. Pevida, Post-combustion CO_2 capture with a commercial activated carbon: comparison of different regeneration strategies, Chemical Engineering Journal 163 (2010) 41–47. doi:10.1016/J.CEJ.2010.07.030.

[16] J. Sreńscek-Nazzal, K. Kiełbasa, Advances in modification of commercial activated carbon for enhancement of CO_2 capture, Applied Surface Science 494 (2019) 137–151. doi:10.1016/j.apsusc.2019.07.108.

[17] R. Ullah, M. Atilhan, S. Aparicio, A. Canlier, C. T. Yavuz, Insights of CO_2 adsorption performance of amine impregnated mesoporous silica (SBA-15) at wide range pressure and temperature conditions, International Journal of Greenhouse Gas Control 43 (2015) 22–32. doi:10.1016/j.ijggc.2015.09.013.

[18] K. Kamarudin, N. Alias, Adsorption performance of MCM-41 impregnated with amine for CO_2 removal, Fuel Processing Technology 106 (2013) 332–337. doi:10.1016/j.fuproc.2012.08.017.

[19] T. T. T. Ngo, E. Besson, E. Bloch, S. Bourrelly, R. Llewellyn, S. Gastaldi, P. L. Llewellyn, D. Gigmes, T. N. T. Phan, One-pot

synthesis of organic polymer functionalized mesoporous silicas, Microporous and Mesoporous Materials 319 (2021) 111036. doi:10.1016/j.micromeso.2021.111036.

[20] K. Wang, H. Shang, L. Li, X. Yan, Z. Yan, C. Liu, Q. Zha, Efficient CO_2 capture on low-cost silica gel modified by polyethyleneimine, Journal of Natural Gas Chemistry 21 (2012) 319–323. doi:10.1016/S1003-9953(11)60371-X.

[21] T. Ghanbari, F. Abnisa, W. M. A. Wan Daud, A review on production of metal organic frameworks (MOF) for CO_2 adsorption, Science of The Total Environment 707 (2020) 135090. doi:10.1016/j.scitotenv.2019.135090.

[22] M. Almáši, V. Zeleňák, R. Gyepes, S. Bourrelly, M. V. Opanasenko, P. L. Llewellyn, J. Čejka, Microporous lead–organic framework for selective CO_2 adsorption and heterogeneous catalysis, Inorganic Chemistry 57 (2018) 1774–1786. doi:10.1021/acs.inorgchem.7b02491, pMID: 29377678.

[23] S.-Y. Lee, S.-J. Park, Determination of the optimal pore size for improved CO_2 adsorption in activated carbon fibers, Journal of colloid and interface science 389 (2013) 230—235. doi:10.1016/j.jcis.2012.09.018.

[24] S. M. Wilson, F. Al-Enzi, V. A. Gabriel, F. H. Tezel, Effect of pore size and heterogeneous surface on the adsorption of CO_2, N_2, O_2, and ar on carbon aerogel, RF aerogel, and activated carbons, Microporous and Mesoporous Materials 322 (2021) 111089. doi:10.1016/j.micromeso.2021.111089.

[25] N. Gargiulo, F. Pepe, D. Caputo, CO_2 adsorption by functionalized nanoporous materials: a review, Journal of nanoscience and nanotechnology 14 (2014) 1811–1822. doi:10.1166/jnn.2014.8893.

[26] P. Muchan, C. Saiwan, M. Nithitanakul, Investigation of adsorption/desorption performance by aminopropyltriethoxysilane grafted onto different mesoporous silica for post-combustion CO_2 capture, Clean Energy 4 (2020) 120–131. doi:10.1093/ce/zkaa003.

[27] C. Cantau, T. Pigot, R. Brown, P. Mocho, M. Maurette, F. Benoit-Marque, S. Lacombe-Lhoste, Photooxidation of dimethylsulfide in the gas phase: A comparison between TiO2-silica and photosensitizer-silica based materials, Applied Catalysis B: Environmental 65 (2006) 77–85. doi:10.1016/j.apcatb.2005.12.019.

[28] Z. V. Faustova, Y. G. Slizhov, Effect of solution ph on the surface morphology of sol–gel derived silica gel, Inorganic Materials 53 (2017) 287–291. doi:10.1134/S0020168517030050.

[29] L. B. Capeletti, I. M. Baibich, I. S. Butler, J. H. Z. dos Santos, Infrared and raman spectroscopic characterization of some organic substituted hybrid silicas, Spectrochimica acta. Part A, Molecular and biomolecular spectroscopy 133 (2014) 619–625. doi:10.1016/j.saa.2014.05.072.

[30] J. L. Blin, C. Carteret, Investigation of the silanols groups of mesostructured silica prepared using a fluorinated surfactant: Influence of the hydrothermal temperature, The Journal of Physical Chemistry C 111 (2007) 14380–14388. doi:10.1021/jp072369h.

[31] R. Al-Oweini, H. El-Rassy, Synthesis and characterization by ftir spectroscopy of silica aerogels prepared using several SI(OR)4 and R"(OR')3 precursors, Journal of Molecular Structure 919 (2009) 140 – 145. doi:10.1016/j.molstruc.2008.08.025.

[32] S. Saliba, P. Ruch, W. Volksen, T. P. Magbitang, G. Dubois, B. Michel, Combined influence of pore size distribution and surface hydrophilicity on the water adsorption characteristics of micro- and mesoporous silica, Microporous and Mesoporous Materials 226 (2016) 221–228. doi:10.1016/j.micromeso.2015.12.029.

[33] L. Zhuravlev, The surface chemistry of amorphous silica. zhuravlev model, Colloids and Surfaces A: Physicochemical and Engineering Aspects 173 (2000) 1 – 38. doi:10.1016/S0927-7757(00)00556-2.

[34] A. A. Christy, New insights into the surface functionalities and adsorption evolution of water molecules on silica gel surface: A study by second derivative near infrared spectroscopy, Vibrational Spectroscopy 54 (2010) 42 – 49. doi:10.1016/j.vibspec.2010.06.003.

[35] Y. Ma, Z. Wang, X. Xu, J. Wang, Review on porous nanomaterials for adsorption and photocatalytic conversion of CO_2, Chinese Journal of Catalysis 38 (2017) 1956–1969. doi:10.1016/S1872-2067(17)62955-3.

[36] S. Kayal, A. Chakraborty, Activated carbon (type maxsorb-iii) and mil-101(cr) metal organic framework based composite adsorbent for higher CH_4 storage and CO_2 capture, Chemical Engineering Journal 334 (2018) 780 – 788. doi:10.1016/j.cej.2017.10.080.

[37] M. Mofarahi, F. Gholipour, Gas adsorption separation of CO_2/CH_4 system using zeolite 5A, Microporous and Mesoporous Materials 200 (2014) 1–10. doi:10.1016/j.micromeso.2014.08.022.

[38] D. Peredo-Mancilla, C. M. Ghimbeu, B.-N. Ho, M. Jeguirim, C. Hort, D. Bessieres, Comparative study of the CH_4/CO_2 adsorption selectivity of activated carbons for biogas upgrading, Journal of Environmental Chemical Engineering 7 (2019) 103368. doi:10.1016/j.jece.2019.103368.

[39] Y. Belmabkhout, R. Serna-Guerrero, A. Sayari, Adsorption of CO_2-containing gas mixtures over amine-bearing pore-expanded MCM-41 silica: Application for CO_2 separation, Adsorption: Journal of the international adsorption society 17 (2011) 395–401. doi:10.1007/s10450-011-9348-0.

[40] S. Ullah, M. A. Bustam, A. G. Al-Sehemi, M. A. Assiri, F. A. Abdul Kareem, A. Mukhtar, M. Ayoub, G. Gonfa, Influence of post-synthetic graphene oxide (go) functionalization on the selective CO_2/CH_4 adsorption behavior of mof-200 at different temperatures; an experimental and adsorption isotherms study, Microporous and Mesoporous Materials 296 (2020) 110002. doi:10.1016/j.micromeso.2020.110002.

[41] M. Z. Ahmad, V. Martin-Gil, T. Supinkova, P. Lambert, R. Castro-Muñoz, P. Hrabanek, M. Kocirik, V. Fila, Novel mmm using CO_2 selective ssz-16 and high-performance 6fda-polyimide for CO_2/CH_4 separation, Separation and Purification Technology 254 (2021) 117582. doi:10.1016/j.seppur.2020.117582.

[42] D. Liang, Y. Hu, Q. Bao, J. Zhang, J. Feng, P. Sun, Y. Ma, H. Zhang, A suitable zeolite rho for separating co2/ch4 in pressure swing adsorption

(psa) process, Inorganic Chemistry Communications 127 (2021) 108547. doi:10.1016/j.inoche.2021.108547.

Highlights

CO_2 capture and CO_2/CH_4 separation by silicas with controlled porosity and functionality

Saphir Venet, Frédéric Plantier, Christelle Miqueu, Ali Shahtalebi, Ross Brown, Thierry Pigot, Patrice Bordat

- Porous silicas with both controlled hydrophilicity and micro-/meso-porosity.
- Materials exhibiting a high separation factor (SF), favouring CO_2 relative to CH_4.
- Degree of residual water favours CO_2 adsorption.
- Easy and cheap one-pot synthesis.
- Gas physisorption favours low cost regeneration.
- Optimal use at low pressures and low CO_2 content.

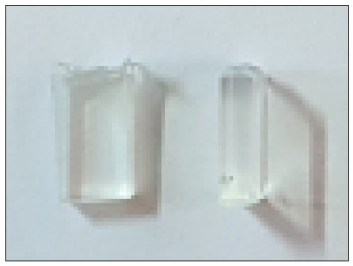

+ CO_2/CH_4 mixture

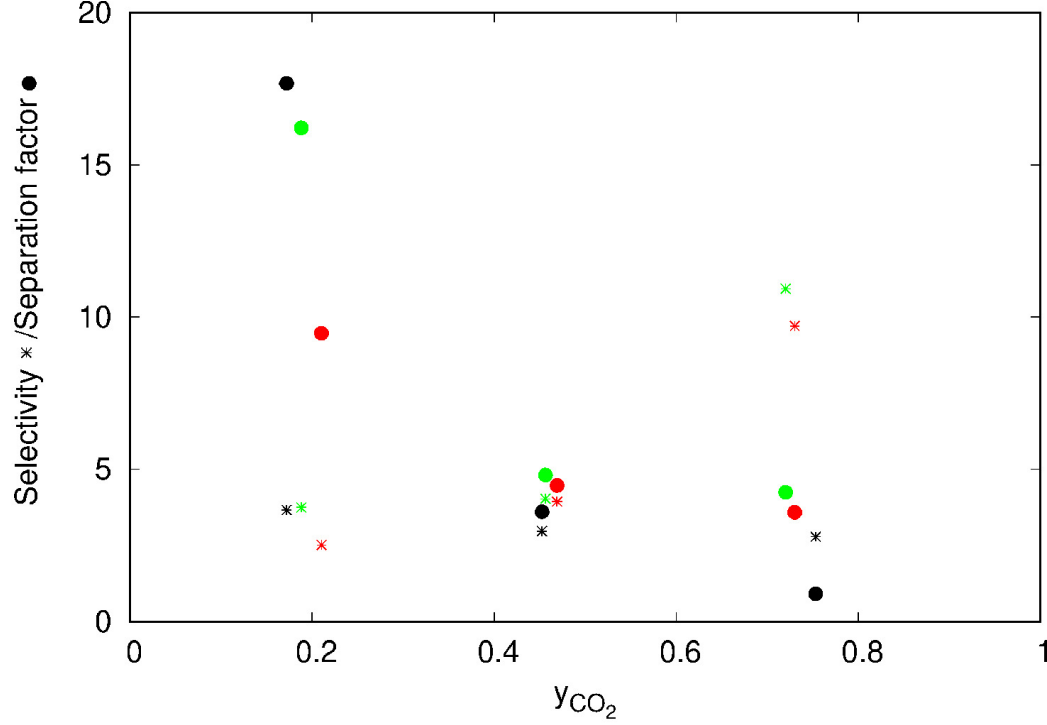

Residual water

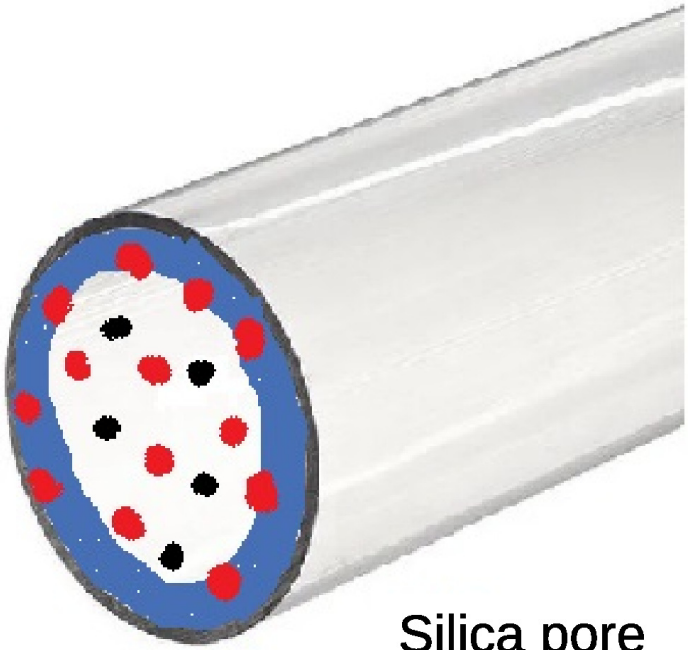

● CO_2

● CH_4

Silica pore